Ionospheric Space Weather

Longitude Dependence and Lower Atmosphere Forcing

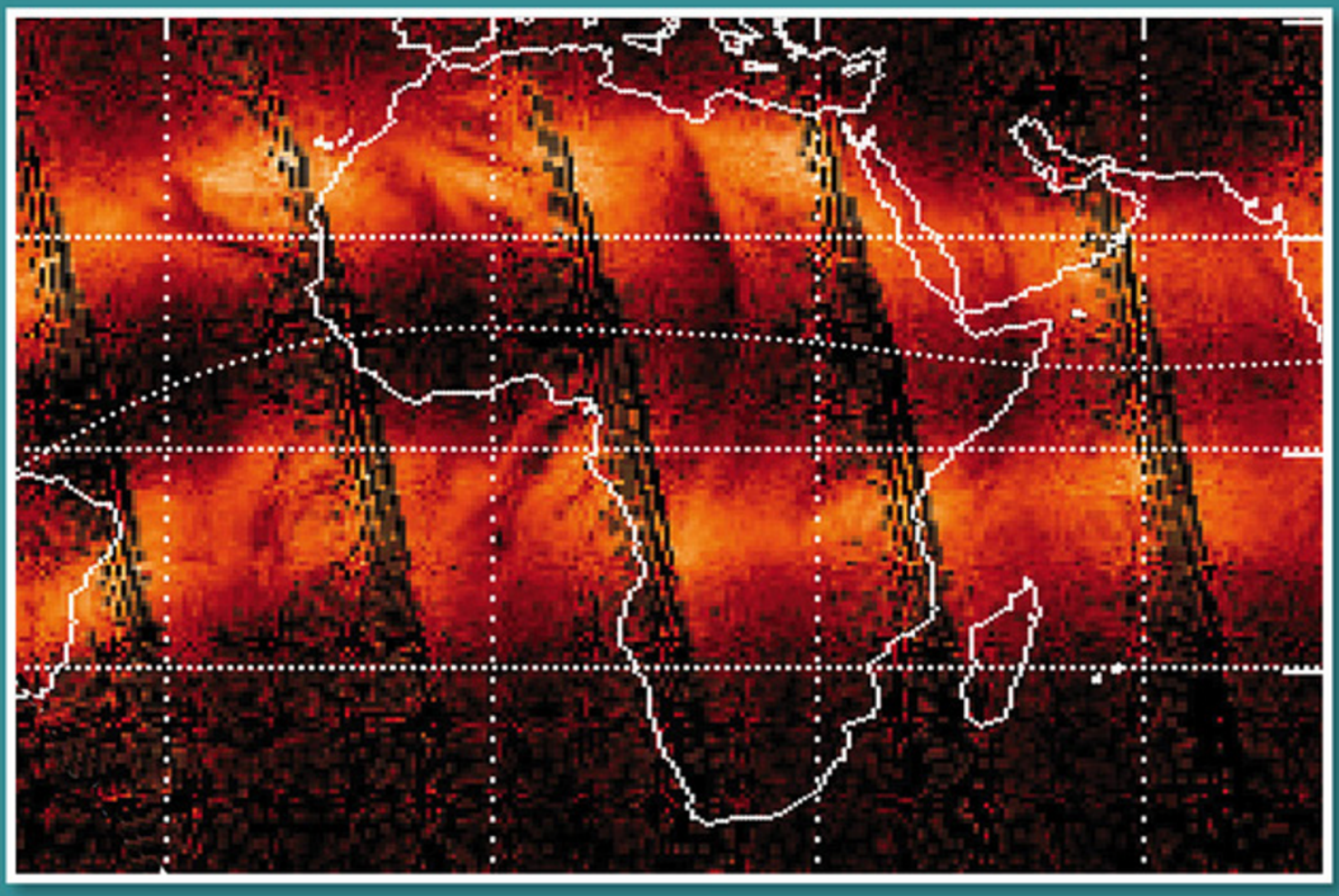

Timothy Fuller-Rowell, Endawoke Yizengaw, Patricia H. Doherty, and Sunanda Basu
Editors

AGU American Geophysical Union

WILEY

Geophysical Monograph Series

177 **Ocean Modeling in an Eddying Regime** *Matthew Hecht and Hiroyasu Hasumi (Eds.)*
178 **Magma to Microbe: Modeling Hydrothermal Processes at Oceanic Spreading Centers** *Robert P. Lowell, Jeffrey S. Seewald, Anna Metaxas, and Michael R. Perfit (Eds.)*
179 **Active Tectonics and Seismic Potential of Alaska** *Jeffrey T. Freymueller, Peter J. Haeussler, Robert L. Wesson, and Göran Ekström (Eds.)*
180 **Arctic Sea Ice Decline: Observations, Projections, Mechanisms, and Implications** *Eric T. DeWeaver, Cecilia M. Bitz, and L.-Bruno Tremblay (Eds.)*
181 **Midlatitude Ionospheric Dynamics and Disturbances** *Paul M. Kintner, Jr., Anthea J. Coster, Tim Fuller-Rowell, Anthony J. Mannucci, Michael Mendillo, and Roderick Heelis (Eds.)*
182 **The Stromboli Volcano: An Integrated Study of the 2002–2003 Eruption** *Sonia Calvari, Salvatore Inguaggiato, Giuseppe Puglisi, Maurizio Ripepe, and Mauro Rosi (Eds.)*
183 **Carbon Sequestration and Its Role in the Global Carbon Cycle** *Brian J. McPherson and Eric T. Sundquist (Eds.)*
184 **Carbon Cycling in Northern Peatlands** *Andrew J. Baird, Lisa R. Belyea, Xavier Comas, A. S. Reeve, and Lee D. Slater (Eds.)*
185 **Indian Ocean Biogeochemical Processes and Ecological Variability** *Jerry D. Wiggert, Raleigh R. Hood, S. Wajih A. Naqvi, Kenneth H. Brink, and Sharon L. Smith (Eds.)*
186 **Amazonia and Global Change** *Michael Keller, Mercedes Bustamante, John Gash, and Pedro Silva Dias (Eds.)*
187 **Surface Ocean–Lower Atmosphere Processes** *Corinne Le Quèrè and Eric S. Saltzman (Eds.)*
188 **Diversity of Hydrothermal Systems on Slow Spreading Ocean Ridges** *Peter A. Rona, Colin W. Devey, Jérôme Dyment, and Bramley J. Murton (Eds.)*
189 **Climate Dynamics: Why Does Climate Vary?** *De-Zheng Sun and Frank Bryan (Eds.)*
190 **The Stratosphere: Dynamics, Transport, and Chemistry** *L. M. Polvani, A. H. Sobel, and D. W. Waugh (Eds.)*
191 **Rainfall: State of the Science** *Firat Y. Testik and Mekonnen Gebremichael (Eds.)*
192 **Antarctic Subglacial Aquatic Environments** *Martin J. Siegert, Mahlon C. Kennicut II, and Robert A. Bindschadler*
193 **Abrupt Climate Change: Mechanisms, Patterns, and Impacts** *Harunur Rashid, Leonid Polyak, and Ellen Mosley-Thompson (Eds.)*
194 **Stream Restoration in Dynamic Fluvial Systems: Scientific Approaches, Analyses, and Tools** *Andrew Simon, Sean J. Bennett, and Janine M. Castro (Eds.)*
195 **Monitoring and Modeling the Deepwater Horizon Oil Spill: A Record-Breaking Enterprise** *Yonggang Liu, Amy MacFadyen, Zhen-Gang Ji, and Robert H. Weisberg (Eds.)*
196 **Extreme Events and Natural Hazards: The Complexity Perspective** *A. Surjalal Sharma, Armin Bunde, Vijay P. Dimri, and Daniel N. Baker (Eds.)*
197 **Auroral Phenomenology and Magnetospheric Processes: Earth and Other Planets** *Andreas Keiling, Eric Donovan, Fran Bagenal, and Tomas Karlsson (Eds.)*
198 **Climates, Landscapes, and Civilizations** *Liviu Giosan, Dorian Q. Fuller, Kathleen Nicoll, Rowan K. Flad, and Peter D. Clift (Eds.)*
199 **Dynamics of the Earth's Radiation Belts and Inner Magnetosphere** *Danny Summers, Ian R. Mann, Daniel N. Baker, and Michael Schulz (Eds.)*
200 **Lagrangian Modeling of the Atmosphere** *John Lin (Ed.)*
201 **Modeling the Ionosphere-Thermosphere** *Jospeh D. Huba, Robert W. Schunk, and George V Khazanov (Eds.)*
202 **The Mediterranean Sea: Temporal Variability and Spatial Patterns** *Gian Luca Eusebi Borzelli, Miroslav Gačić, Piero Lionello, and Paola Malanotte-Rizzoli (Eds.)*
203 **Future Earth - Advancing Civic Understanding of the Anthropocene** *Diana Dalbotten, Gillian Roehrig, and Patrick Hamilton (Eds.)*
204 **The Galápagos: A Natural Laboratory for the Earth Sciences** *Karen S. Harpp, Eric Mittelstaedt, Noémi d'Ozouville, and David W. Graham (Eds.)*
205 **Modeling Atmospheric and Oceanic Flows: Insights from Laboratory Experiments and Numerical Simulations** *Thomas von Larcher and Paul D. Williams (Eds.)*
206 **Remote Sensing of the Terrestrial Water Cycle** *Venkat Lakshmi (Eds.)*
207 **Magnetotails in the Solar System** *Andreas Keiling, Caitríona Jackman and Peter Delamere (Eds.)*
208 **Hawaiian Volcanoes: From Source to Surface** *Rebecca Carey, Valerie Cayol, Michael Poland, and Dominique Weis (Eds.)*
209 **Sea Ice: Physics, Mechanics, and Remote Sensing** *Mohammed Shokr and Nirmal Sinha (Eds.)*
210 **Fluid Dynamics in Complex Fractured-Porous Systems** *Boris Faybishenko, Sally M. Benson, and John E. Gale (Eds.)*
211 **Subduction Dynamics: From Mantle Flow to Mega Disasters** *Gabriele Morra, David A. Yuen, Scott King, Sang Mook Lee, and Seth Stein (Eds.)*
212 **The Early Earth: Accretion and Differentiation** *James Badro and Michael Walter (Eds.)*
213 **Extreme Events** *Mario Chavez, Michael Ghil, and Jaime Urrutia Fucugauchi (Eds.)*
214 **Global Vegetation Dynamics** *Dominique Bachelet and David Turner (Eds.)*
215 **Auroral Dynamics and Space Weather** *Yongliang Zhang and Larry Paxton (Eds.)*
216 **Low-Frequency Waves in Space Plasmas** *Andreas Keiling, Dong-Hun Lee, and Valery M. Nakariakov (Eds.)*
217 **Deep Earth** *Hidenori Terasaki and rebecca Fischer (Eds.)*
218 **Integrated Imaging of the Earth** *Max Moorkamp, Peter Lelièvre, Niklas Linde, and Amir Khan (Eds.)*
219 **Plate Boundaries and Natural Hazards** *Joao Duarte and Wouter Schellart (Eds.)*

Geophysical Monograph 220

Ionospheric Space Weather

Longitude and Hemispheric Dependences and Lower Atmosphere Forcing

Timothy Fuller-Rowell
Endawoke Yizengaw
Patricia H. Doherty
Sunanda Basu
Editors

This Work is a copublication between the American Geophysical Union and John Wiley and Sons, Inc.

AGU
American Geophysical Union

WILEY

This Work is a copublication between the American Geophysical Union and John Wiley & Sons, Inc.

Published under the aegis of the AGU Publications Committee

Brooks Hanson, Director of Publications
Robert van der Hilst, Chair, Publications Committee

Published by John Wiley & Sons, Inc., Hoboken, New Jersey
Published simultaneously in Canada

Library of Congress Cataloging-in-Publication Data is available.

ISBN: 978-1-118-92920-9

Cover images: Front Cover: Figure shows images of ionospheric irregularities over Africa as seen in airglow depletions. The dark patches within the brighter equatorial "arcs," on either side of the geomagnetic equator (dotted curved line), indicate where communication signals would be lost (figure courtesy of Larry Paxton, Applied Physics Laboratory). Back cover: (left) Ground-based instrument coverage in Africa seven years ago and (right) the current ground-based instrumentation in Africa.

Printed in the United States of America

10 9 8 7 6 5 4 3 2 1

CONTENTS

CONTRIBUTORS

Gebregiorgis Abraha
Department of Physics, Addis Ababa University
Addis Ababa, Ethiopia;
Department of Physics
Mekele University
Mekele, Ethiopia

Rasaq A. Adeniji-Adele
Department of Physics
Lagos State University
Ojo, Lagos, Nigeria

Andrew O. Akala
Department of Physics
University of Lagos
Akoka, Lagos, Nigeria

David Anderson
Cooperative Institute for Research in
Environmental Sciences (CIRES)
University of Colorado at Boulder
Boulder, Colorado, USA; *and*
Space Weather Prediction Center (SWPC)
National Oceanic and Atmospheric
Administration (NOAA)
Boulder, Colorado, USA

Joseph Baker
Bradley Department of Electrical and
Computer Engineering
Virginia Tech
Blacksburg, Virginia, USA

Athanasios Boudouridis
Center for Space Plasma Physics
Space Science Institute
Boulder, Colorado, USA

Dalia Burešová
Department of Aeronomy
Institute of Atmospheric Physics
Academy of Sciences of the Czech Republic (ASCR)
Prague, Czech Republic

Brett A. Carter
Institute for Scientific Research
Boston College
Chestnut Hill, Massachusetts, USA

Peter Chi
Department of Earth and Space Sciences
University of California, Los Angeles
Los Angeles, California, USA

Anthea J. Coster
Haystack Observatory
Massachusetts Institute of Technology
Westford, Massachusetts, USA

Baylie Damtie
Department of Physics
Washera Geospace and Radar Science
Laboratory
Bahir Dar University
Bahir Dar, Ethiopia

Vafi Doumbia
Laboratoire de Physique de l'Atmosphère
Université Félix Houphouët-Boigny
Abadji Kouté, Abidjan, Côte d'Ivoire

Florence M. D'ujanga
Department of Physics
Makerere University
Kampala, Uganda

Francis G. Eparvier
Laboratory for Atmospheric and Space Physics
University of Colorado at Boulder
Boulder, Colorado,
USA

Philip J. Erickson
Haystack Observatory
Massachusetts Institute of Technology
Westford, Massachusetts, USA

Tzu-Wei Fang
Cooperative Institute for Research in
Environmental Sciences (CIRES)
University of Colorado at Boulder
Boulder, Colorado, USA; *and*
Space Weather Prediction Center (SWPC)
National Oceanic and Atmospheric
Administration (NOAA)
Boulder, Colorado, USA

Daniel J. Fisher
Department of Electrical and Computer Engineering
University of Illinois at Urbana-Champaign
Urbana, Illinois, USA

Olanike O. Folarin
Ionospheric & Space Physics Laboratory
Department of Physics
University of Lagos, Akoka, Nigeria

John C. Foster
Haystack Observatory
Massachusetts Institute of Technology
Westford, Massachusetts, USA

Timothy J. Fuller-Rowell
Cooperative Institute for Research in Environmental Sciences (CIRES)
University of Colorado at Boulder
Boulder, Colorado, USA; *and*
Space Weather Prediction Center (SWPC)
National Oceanic and Atmospheric Administration (NOAA)
Boulder, Colorado, USA

Oswald Didier Franck Grodji
Laboratoire de Physique de l'Atmosphère
Université Félix Houphouët-Boigny
Abadji Kouté, Abidjan, Côte d'Ivoire

Roderick A. Heelis
William Hanson Center for Space Sciences
University of Texas at Dallas
Richardson, Texas, USA

Klemens Hocke
Institute of Applied Physics
University of Bern
Bern, Switzerland

Peter Hoffmann
Leibniz Institute of Atmospheric Physics
Rostock University
Kühlungsborn, Germany

Mohammed Mainul Hoque
Institute of Communications and Navigation
German Aerospace Center (DLR)
Neustrelitz, Germany

Joseph D. Huba
Plasma Physics Division
Naval Research Laboratory
Washington, D.C., USA

Enerst E. Iheonu
Department of Physics
Lagos State University
Ojo, Lagos, Nigeria

Norbert Jakowski
Institute of Communications and Navigation
German Aerospace Center (DLR)
Neustrelitz, Germany

Gebreab Kidanu
Department of Physics, Addis Ababa University
Addis Ababa, Ethiopia; *and*
University of Texas at Dallas
Dallas/Fort Worth, Texas, USA

Jan Laštovička
Department of Aeronomy
Institute of Atmospheric Physics
Academy of Sciences of the Czech Republic (ASCR)
Prague, Czech Republic

Jonathan J. Makela
Department of Electrical and Computer Engineering
University of Illinois at Urbana-Champaign
Urbana, Illinois, USA

James P. Mason
Laboratory for Atmospheric and Space Physics
University of Colorado at Boulder
Boulder, Colorado, USA

Vivien Matthias
Leibniz Institute of Atmospheric Physics
Rostock University
Kühlungsborn, Germany

Gizaw Mengistu Tsidu
Department of Physics, Addis Ababa University, Addis Ababa, Ethiopia; Karlsruhe Institute of Technology (KIT), Institute for Meteorology and Climate Research (IMK-ASF), Karlsruhe, Germany; *and*
Department of Earth and Environmental Sciences, Botswana International University of Science and Technology (BIUST)
Palapye, Botswana

John W. Meriwether
Department of Physics and Astronomy
Clemson University
Clemson, South Carolina, USA

Mark B. Moldwin
Atmospheric, Oceanic, and Space Science (AOSS)
University of Michigan
Ann Arbor, Michigan, USA

Chigomezyo M. Ngwira
Department of Physics
Catholic University of America
Washington, D.C., USA; *and*
Space Weather Laboratory
NASA Goddard Space Flight Center
Greenbelt, Maryland, USA

Melessew Nigussie
Department of Physics
Washera Geospace and Radar Science Laboratory
Bahir Dar University
Bahir Dar, Ethiopia

Aghogho Ogwala
Department of Physics
Lagos State University
Ojo, Lagos, Nigeria

Eugene O. Onori
Department of Physics
Lagos State University
Ojo, Lagos, Nigeria

Phillip Opio
Department of Physics
Makerere University
Kampala, Uganda

Edgardo E. Pacheco
Instituto Geofísico del Perú
Jicamarca Radio Observatory, Lima
Lima, Peru

A. Babatunde Rabiu
Center for Atmospheric Research (CAR)
National Space Research and Development Agency
Anyigba, Nigeria

Sandro M. Radicella
Telecommunication/ICT for Development Laboratory
Abdu Salam International Center for Theoretical Physics (ICTP)
Trieste, Italy

J. Michael Ruohoniemi
Bradley Department of Electrical and Computer Engineering
Virginia Tech
Blacksburg, Virginia, USA

Ludger Scherliess
Center for Atmospheric and Space Sciences
Utah State University
Logan, Utah, USA

Robert Sheehan
Institute for Scientific Research
Boston College
Newton, Massachusetts, USA

Emmanuel O. Somoye
Department of Physics
Lagos State University
Ojo, Lagos, Nigeria

Simone Studer
Institute of Applied Physics
University of Bern
Bern, Switzerland

Evan G. Thomas
Bradley Department of Electrical and Computer Engineering
Virginia Tech
Blacksburg, Virginia, USA

Justin S. Tsu
Atmospheric, Oceanic, and Space Science (AOSS)
University of Michigan
Ann Arbor, Michigan, USA

Francis Twinomugisha
Department of Physics
Makerere University
Kampala, Uganda

Teiji Uozumi
International Center for Space Weather Science and Education (ICSWSE)
Kyushu University
Fukuoka, Japan

Cesar E. Valladares
Institute for Scientific Research
Boston College
Newton, Massachusetts, USA

Houjun Wang
Cooperative Institute for Research in Environmental Sciences (CIRES)
University of Colorado at Boulder
Boulder, Colorado, USA; *and*
Space Weather Prediction Center (SWPC)
National Oceanic and Atmospheric Administration (NOAA)
Boulder, Colorado, USA

James M. Weygand
Institute of Geophysics and Planetary Physics
University of California, Los Angeles
Los Angeles, California, USA

Thomas N. Woods
Laboratory for Atmospheric and Space Physics
University of Colorado at Boulder
Boulder, Colorado, USA

Endawoke Yizengaw
Institute for Scientific Research
Boston College
Chestnut Hill, Massachusetts, USA

Akimasa Yoshikawa
Earth and Planetary Sciences
Kyushu University
Fukuoka, Japan;
International Center for Space Weather Science and Education (ICSWSE)
Kyushu University
Fukuoka, Japan

Eftyhia Zesta
Heliophysics Science Division
NASA Goddard Space Flight Center
Greenbelt, Maryland, USA

PREFACE

This monograph is the outcome of an American Geophysical Union (AGU) Chapman Conference, "Longitude and Hemispheric Dependence of Space Weather," held in Addis Ababa, Ethiopia, in 2012. The meeting was the culmination of a series of space science meetings and summer schools held in Africa over the past 8 yr. Five years earlier, in 2007, a space science meeting was held in the same city as part of the International Heliophysical Year (IHY). IHY was an effort to reinvigorate the international collaboration in geophysics under the umbrella of the United Nations, a tradition that began 50 yr earlier with the International Geophysical Year (IGY). Subsequent meetings were held in Zambia in 2009. IHY was superseded by the International Space Weather Initiative (ISWI), again under the umbrella of the United Nations. In recognition of the unprecedented achievement of the space science development in Africa, AGU held a prestigious International Chapman Conference in Africa, the first of its kind in the space sciences. One of the highlights of the meeting was formally establishing the African Geophysical Society (AGS).

Although much progress has been made in the study of ionospheric space weather in the last decade, many gaps remain in our global understanding of some of the fundamental processes. For instance, the global electrodynamics that governs the formation of equatorial ionospheric irregularities, which is of practical importance impacting satellite communication and navigation, is still not well understood, hindered by uneven distribution of ground-based instruments. Questions remain, such as, are ionospheric space weather effects the same over the American, African, and Asian longitude sectors, or are they different, and if so why? Observations from instruments on board LEO satellites (e.g., the Communications/Navigation Outage Forecast System C/NOFS), indicate that there is, in fact, strong longitude dependence. Ionospheric irregularities for some reason appear to be more prevalent over the African continent, but it is unclear why. The front cover of this monograph shows images of equatorial plasma bubbles in the ionosphere over Africa obtained from the GUVI instrument on the TIMED satellite using airglow emissions at 135.6 nm (courtesy of Larry Paxton, JHU-APL). The regions of depleted airglow within the brighter equatorial "arcs" are the regions where satellite signals would be scintillated and communication could be lost. Addressing the reason for the longitudinal differences was one of the foci of the Chapman Conference.

One of the reasons for the barrier to understanding some of these longitude dependences is the uneven distribution of ground-based instruments worldwide. Space-based observations, such as C/NOFS, contribute a lot, but there is no substitute for the extended continuous observations from the ground. An obvious step forward in addressing some of the questions on continental and longitude scales was to improve ground-based observations over Africa, an extensive region with a dearth of observations. The Chapman Conference and other meetings held in Africa were a means of focusing attention on an extensive geographic region where observations were critically needed to address some of the fundamental questions of the physical processes driving the ionosphere locally and globally.

The concerted effort over the past 8 yr to try to develop the observational infrastructure has resulted in the situation depicted on the back cover of this monograph. The comparison of ground-based distribution of space science instrumentations (including GNSS receivers, magnetometers, ionosondes, and radars) over Africa in 2007 (left panel) with 2012 (right panel), shows the significant change. There are now many more ground-based ionospheric electron-content observations from GNSS receivers, and plasma drifts estimation from magnetometer observations, that can tackle some of the outstanding scientific questions.

The Chapman Conference was an ideal opportunity to hear about some of these new observations over Africa, which are starting to confirm that the occurrence of ionospheric irregularities are indeed more frequent and stronger in this longitude sector. One possibility that emerged as the cause is the very symmetric shape of the geomagnetic equator over African longitudes, compared with the American sector where it is very distorted with steep tilts in declination and offsets compared with the geographic equator. Another possibility is the size of the landmass in Africa, which has the longest section of the geomagnetic equator over land.

In addition to highlighting the longitude dependence, the meeting explored the impact of the lower atmosphere on space weather. When the Sun is active and a large solar flare or geomagnetic storm is in progress, the Sun is certainly dominant. However, a lot of the day-to-day variability in near-Earth space weather, and some of the longitude dependence, is driven by tropospheric weather and the changing synoptic weather patterns. This may be one of the reasons the African continent experiences

different space weather phenomena. It is clear that "tropospheric" weather and lower atmosphere dynamics have a definite, clear, and coherent impact on space weather in the ionosphere. This means that regular terrestrial weather, such as the strength of tropical convection, which is known to have large ocean/land differences, may be producing very different background conditions in the upper atmosphere and ionosphere. The Chapman Conference brought African and international scientists together to discuss these issues.

Waves and tides originating in the low atmosphere and propagating upward into the upper atmosphere and ionosphere were important topics of discussion and are part of this monograph. The waves from the lower atmosphere impacting space weather include gravity waves (GW), migrating and nonmigrating tidal waves, and planetary waves (PW). The tropospheric origin of GWs with periods of about 20 min up to several hours and vertical wavelengths of about 100–300 km can propagate rapidly toward higher altitudes and modulate ionospheric electrodynamics and density distributions. Secondary GWs, which may be generated in the lower thermosphere, have higher phase speeds and larger spatial scales. They are able to penetrate well into ionospheric altitudes and may initiate the growth of ionospheric irregularities, generated by the Rayleigh-Taylor instability. The ionospheric irregularities are often referred to as equatorial plasma bubbles (EPBs). Ionospheric modeling of centimeter- to kilometer-scale low-latitude ionospheric irregularities suggests that poleward neutral winds tend to stabilize the ionospheric plasma, whereas equatorward winds tend to destabilize. It was also reported at the meeting that the zonal wind is responsible for the formation of the longitudinal wavenumber-4 structures, which have been observed at all universal times. The geomagnetic declination also contributes significantly to the growth of plasma bubbles.

Another important space-weather impact is geomagnetically induced currents in electrical distribution systems and pipelines. The focus is normally on middle and high latitudes where the ionospheric currents are expected to be the strongest. Observations reported at the Chapman Conference and in this monograph show that the equatorial electrojet (EEJ) as well as storm sudden commencement (SSC) currents can give rise to rapid changes in the horizontal component of Earth's magnetic field (dB_H/dt), with values of hundreds of nT/min during storm periods, which is comparable to the March 1989 auroral electrojet of 500 nT/min. These large geomagnetic responses to the EEJ current can cause large induced currents (GICs) and hence damage power plants located near the magnetic equator. The other perception is that power grids are of smaller scale and less well developed at low latitudes, implying GICs would have less of an impact in the region. However, recent economic development data show that countries under the EEJ region are some of the fastest growing economies in the world and are developing large-scale power transmission systems, which can be easily exposed to power failures during large geomagnetic or space weather disturbances.

The Chapman Conference was successful in all aspects. Collaborations were established, and, more important, students were exposed to the field of space science and had opportunities to have one-on-one discussions with established international scientists. International Chapman Conferences such as this make a valuable contribution to worldwide scientific research and outreach programs.

To develop space science research infrastructure within Africa, space science educational infrastructure also needs to be developed to support the long-term operation and use of the science instrumentation. One way to address this concern is to increase and facilitate a strong interaction between scientists from developed countries and African young professors and postgraduate students. In response to these needs, several other international workshops/conferences and summer schools have already been conducted across the African continent.

With the increasing reliance on technology, the impact of space weather on engineered systems will certainly increase unless suitable protective measures are taken. Understanding the physics behind space weather and improving the forecasting is a major objective of the space-science community. It is well recognized that many space-weather impacts, especially on communications systems, arise from structures in the ionosphere. The equatorial ionosphere in particular is one of the most complex and is host to numerous instabilities and interactions, with many unresolved questions regarding its dynamics and variability. Radio waves, either transmitted through the ionosphere for satellite communication and navigation or reflected off the ionosphere for high-frequency (HF) and radar applications, are all impacted by ionospheric variability and structure. Ionospheric irregularities, or plasma bubbles, occurring at low latitudes are one such source of interference. These irregularities cause scintillations on satellite-radio transmissions resulting in information loss in communications, as well as degradation in positioning and navigation used in aviation and maritime industries.

The compilation of papers in this monograph covers various aspects of the physics of the system, and the mechanisms that control ionospheric space weather, in a combination of tutorial-like and focused articles that will be of value to the upper atmosphere scientific community in general and to the ongoing global magnetosphere-ionosphere-thermosphere (MIT) modeling effort in particular. A number of articles from each science theme describe details of the physics behind each phenomenon that help to solve the complexity of the MIT system.

Since the monograph is an outcome of the research presented at this first international space science Chapman Conference held in Africa, it has further provided an opportunity and motivation to the African scientists to communicate their research results with the international community using the volume as a vehicle. In addition, the meeting and this conference volume will greatly enhance the space-science education and research interest in the African continent and around the world.

Ionospheric Space Weather includes articles from six science themes that were discussed at the Chapman Conference in 2012. These include:

- Hemispherical dependence of magnetospheric energy injection and the thermosphere-ionosphere response
- Longitude and hemispheric dependence of storm-enhanced densities (SED)
- Response of the thermosphere and ionosphere to variability in solar radiation
- Longitude spatial structure in total electron content and electrodynamics
- Temporal response to lower-atmosphere disturbances
- Ionospheric irregularities and scintillation

Ionospheric Space Weather: Longitude and Hemispheric Dependences and Lower Atmosphere Forcing will be useful to both active researchers and advanced graduate students in the fields of physics, geophysics, and engineering, especially those who are keen to acquire a global understanding of ionospheric phenomena, including observational information from all longitude sectors across the globe.

The editors would also like to take this opportunity to thank the many people that devoted their time to carefully reviewing the manuscripts for this volume. We would also like to thank Karen O'Loughlin for checking all the manuscripts for internal consistency and for ensuring completeness of the index.

Timothy Fuller-Rowell
Endawoke Yizengaw
Patricia H. Doherty
Sunanda Basu

Part I
Hemispherical Dependence of Magnetospheric Energy Injection and the Thermosphere-Ionosphere Response

1

Interhemispheric Asymmetries in Magnetospheric Energy Input

Eftyhia Zesta,[1] Athanasios Boudouridis,[2] James M. Weygand,[3] Endawoke Yizengaw,[4] Mark B. Moldwin,[5] and Peter Chi[6]

ABSTRACT

Energy transfer from the solar wind to the magnetosphere-ionosphere-thermosphere system occurs via multiple routes with coupling efficiency depending on the Interplanetary Magnetic Field (IMF), solar wind, and the magnetosphere prior state. The energy is not always released in the two hemispheres symmetrically. Ultra low frequency (ULF) waves are the natural perturbations of the magnetosphere and the plasma in it, thus constituting an excellent diagnostic of how energy is transported throughout this complex system. We explore the question of how energy is deposited asymmetrically in the two hemispheres by studying (1) asymmetries of auroral currents and (2) asymmetries in ULF wave power at magnetically conjugate locations. We also construct a Southern Hemisphere auroral electrojet (AE) index and compare it with the standard AE index. We find that while in general the north and south electrojet indices correlate well, significant asymmetries occur frequently, primarily in the local midnight region. We also find that at low latitudes and midlatitudes the north-to-south wave-power ratio exhibits clear annual variation with a systematic offset: the Northern Hemisphere always has stronger power than the Southern Hemisphere. This systematic asymmetry is also seen in the ionospheric total electron content (TEC), implying a close link.

Key Points:
Interhemispheric asymmetries in ULF wave power and total electron content
A southern auroral electrojet index and comparison with the standard AE index
Interhemispheric asymmetries between northern and southern auroral electrojet indices

Key Terms: equatorial ionosphere, equatorial electrojet (EEJ), ground-induced currents (GIC)

[1]*Heliophysics Science Division, NASA Goddard Space Flight Center, Greenbelt, Maryland, USA*
[2]*Center for Space Plasma Physics, Space Science Institute, Boulder, Colorado, USA*
[3]*Institute of Geophysics and Planetary Physics, University of California, Los Angeles, Los Angeles, California, USA*
[4]*Institute for Scientific Research, Boston College, Chestnut Hill, Massachusetts, USA*
[5]*Atmospheric, Oceanic, and Space Science (AOSS), University of Michigan, Ann Arbor, Michigan, USA*
[6]*Department of Earth and Space Sciences, University of California, Los Angeles, Los Angeles, California, USA*

1.1. INTRODUCTION

It is generally assumed that most of the dynamic geospace phenomena, like magnetic storms and substorms, develop in unison in both Northern and Southern Hemispheres, typically starting in the polar regions. High-latitude geomagnetic field lines carry a load of field-aligned currents (FACs) and electromagnetic waves directly from the magnetopause, where the heavy coupling from the solar wind to the magnetosphere occurs, down to the ionosphere and thermosphere, depositing energy in the form

Ionospheric Space Weather: Longitude and Hemispheric Dependences and Lower Atmosphere Forcing, Geophysical Monograph 220, First Edition. Edited by Timothy Fuller-Rowell, Endawoke Yizengaw, Patricia H. Doherty, and Sunanda Basu.

of Poynting flux that heats both the ionosphere and neutral atmosphere. A part of the solar-wind energy gets processed in the magnetotail first, and is ultimately deposited in the ionosphere via both currents and electromagnetic waves, but also particle precipitation that can form bright auroras. Another part of the solar-wind energy is stored in the inner magnetosphere and couples to the mid-latitude and low-latitude ionosphere through electric fields, waves, and particle precipitation. During equinox, it is generally assumed that the load of currents and waves is approximately symmetric into the north and south polar ionospheres, but becomes quite asymmetric when either of the poles is tilted toward the Sun during the solstices [e.g., *Wu et al.*, 1991]. At those times, the uneven solar EUV illumination becomes a controlling factor for the asymmetric ionospheric conductivity in the two polar regions, leading to large asymmetries in the electrodynamic coupling with the magnetosphere and the amount of heating that is transferred to the neutrals.

While seasonal effects are strong drivers of interhemispheric asymmetries, other factors, such as the dipole tilt with respect to the rotation axis, the Interplanetary Magnetic Field (IMF) orientation, local magnetic field structures, and even atmospheric dynamics, can and do play a significant role in the strong interhemispheric asymmetries that are observed at all latitudes. For example, *Knipp et al.* [2000] showed significant difference in the amount of energy input, both from Joule heating and precipitation, in the two hemispheres during an 11-hr interval in May 1999. *Knipp et al.* argued that the large asymmetries were due to both the Northern Hemisphere sunward tilt and to the IMF orientation.

The tilt and offset of the dipolar part of the Earth's magnetic field places the polar caps at different geographic latitudes resulting in lower geomagnetic latitudes seeing 24 hr darkness in the Southern Hemisphere in the Americas longitude sector than in the Northern Hemisphere during northern summer, further exacerbating conductivity and electrodynamic asymmetries. *Cnossen and Richmond* [2012] demonstrated via modeling that the tilt angle of the geomagnetic dipole is a strong controlling factor in the distribution of Joule heating in the high latitudes and in the neutral temperature and winds. *Förster and Cnossen* [2013] took this work further to demonstrate, again via modeling, the effect the nondipolar components of the Earth's magnetic field have in interhemispheric asymmetries. They found that while the effect in the large-scale plasma convection was rather small, the effect on the neutral winds was substantial.

It is a common assumption, particularly in simulations, that auroral activity, brightenings, and dynamics in the Northern and Southern hemispheres are a mirror image of each other, based on the assumption that the magnetospheric processes are similarly mapped down to the two polar regions, and the source particles are evenly distributed along the same field lines to the two ionospheres. While seasonal differences have been statistically reported [e.g., *Newell et al.*, 1996; *Liou et al.*, 2001], the global patterns of precipitation are typically assumed symmetric in the two hemispheres.

The substorm phenomenon is perhaps the most common and dramatic nightside auroral intensification. All of today's models of substorms are based mostly on Northern Hemisphere observations and assume conjugacy between hemispheres. Studies of the conjugacy (or not) of substorm onset and its dynamics have primarily relied on ground or aircraft imagers and magnetometers located at conjugate points [e.g., *Belon et al.*, 1969; *Stenbaek-Nielsen et al.*, 1972, 1973; *Hajkowicz*, 2006; *Motoba et al.*, 2014]. Studies based on older instrumentation and limited cases found good conjugacy between of the auroras for both quiet and active conditions [e.g., *Belon et al.*, 1969; *Stenbaek-Nielsen et al.*, 1972], but new studies with more sophisticated instrumentation and longer statistical studies have begun to demonstrate interhemispheric asymmetries in larger and smaller scale size structures [e.g., *Hajkowicz*, 2006; *Laundal and Østgaard*, 2009; *Motoba et al.*, 2014; *Weygand et al.*, 2014a]. Fewer studies were able to use satellite auroral imagery on few fortuitous conjunctions [*Ostgaard et al.*, 2004, 2007; *Frank and Sigwarth*, 2003; *Sato et al.*, 2012]. Many of these studies have reported significant asymmetries, both in the location and timing of the substorm onset [e.g., *Morioka et al.*, 2011; *Sato et al.*, 1998; *Weygand et al.*, 2014b]. *Kivelson et al.* [1996] and *Ostgaard et al.* [2004, 2007] found that the north-south displacement of the onset systematically depends on the IMF B_y sign and magnitude.

Frank and Sigwarth [2003] presented the first simultaneous satellite observations of a substorm onset (observed by Polar VIS camera at both hemispheres simultaneously). They found a 1–2 min delay in the occurrence of the onset between the two hemispheres and that traditional mapping would place the source of the onset from the two hemispheres on significantly different locations on the tail. Clearly, our understanding of how tail dynamics couple down to the ionosphere is incomplete.

While there are many works looking at the asymmetries of substorm auroral dynamics, there are limited studies that demonstrate asymmetric auroral features and energy input for less active periods. *Shi et al.* [2012] showed that the cusp location moved asymmetrically between the two hemispheres while the dipole tilt angle increased, resulting at the cusp forming at different latitudes at the two hemispheres. *Fillingim et al.* [2005] used coincidental observations from IMAGE FUV and Polar UVI and observed significant asymmetries in the structure of the afternoon aurora, which they attributed to IMF B_y effects. *Stubbs et al.* [2005] looked at the relative location

of the complete auroral oval from simultaneous IMAGE and Polar observations from both hemispheres and found that not only IMF B_y, but also B_x, affect the displacement of the oval in the two hemispheres. *Motoba et al.* [2012] recently analyzed detailed observations of auroral beads from conjugate all-sky auroral imagers that occurred ~15 min before a substorm onset. They found that the beads developed simultaneously and with great similarity in the two hemispheres.

There is evidence that the auroral electrojets exhibit seasonal asymmetries [*Wu et al.*, 1991], although most studies depend on spatially limited magnetometer chains, or individual conjugate pairs of magnetometers. *Wu et al.* [1991] reported that the substorm westward electrojet flows at higher latitudes in the winter hemisphere than in the summer hemisphere by as much as 4°. The interhemispheric asymmetries of the auroral electrojets are likely a direct result of the interhemispheric asymmetries in field-aligned currents (FACs). Theoretical studies have predicted that conductivity differences between the winter and summer hemispheres will create a set of interhemispheric FACs (IHCs) [*Benkevich et al.*, 2000]. The IHCs flow from one hemisphere to the other along highly conductive magnetic field lines connecting the two conjugate auroral zones and have the effect of redistributing the ionospheric currents in the two hemispheres with significantly different conductivities. Although IHCs have been modeled from first principles [*Benkevich et al.*, 2000; *Lyatskaya et al.*, 2014a; 2014b], they have yet to be observed, primarily due to lack of the necessary observations, that is, coincidental observations of FACs from both hemispheres on the same local time sector. Our lack of conjugate observations on the global scale has clearly limited our understanding of dynamic phenomena like substorms.

This is where more recent data assembly techniques like AMPERE [*Anderson et al.*, 2002] and SuperMAG [*Gjerloev*, 2012] can help break through the prior observational limitation. The Active Magnetosphere and Planetary Electrodynamics Response Experiment (AMPERE) Science Data Center is a facility that uses magnetometer data from the 66 IRIDIUM satellites and sophisticated algorithms to provide the global FAC patterns every 10 min [*Anderson et al.*, 2002]. SuperMAG [*Gjerloev*, 2012] is a worldwide collaboration of ground magnetometer chains that operate more than 300 magnetometers and provides easy access to validated ground magnetic field perturbations in the same coordinate system and identical time resolution with a common baseline removal approach. Products like the global equivalent ionospheric currents are also provided. It is now possible to support large-scale interhemispheric studies.

Here we focus on two specific topics. First, in Section 1.2, we discuss interhemispheric asymmetries of the auroral electrojets as a means of understanding how dynamic phenomena develop differently in the two hemispheres. Then, in Section 1.3, we discuss interhemispheric asymmetries of the power of ultra low frequency (ULF) waves at low latitudes and midlatitudes and see what the role of the ionosphere is in such asymmetries. We end with a brief summary.

1.2. ASYMMETRIES IN HIGH-LATITUDE DYNAMICS AND THE AURORAL CURRENTS

The auroral elecrojet (AE) index (*Davis and Sugiura*, 1966) is traditionally calculated from a set of 10–13 ground magnetometer stations located around the typical northern auroral oval location (between 60° and 70° geomagnetic latitude). There is no Southern Hemisphere AE index because there is not sufficient station coverage from the southern auroral oval. The AE index is used as the most common indicator of global geomagnetic activity and it is well correlated with the strength of the auroral electrojets and also with auroral activity. It is typically used for identifying the occurrence, onset, and strength of a substorm. Considering the evidence for significant differences in both the location and timing of the auroral substorm onset and dynamics, it follows that the AE index should exhibit similar asymmetries.

Efforts to calculate a southern AE index are few, given the limited landmass availability at the appropriate latitudes in the Southern Hemisphere. *Maclennan et al.* [1991] used 22 available ground magnetometer stations from Antarctica to calculate a southern AE (SAE) index for 7 days in June 1982 and compare it with the northern World Data Center (WDC) AE. They found that the WDC AE was consistently stronger than the SAE index, which was likely due to seasonal effects. The *Maclennan et al.* [1991] study, however, included stations within a wide latitude range, from 50° to 90° magnetic, thus almost certainly including stations that at any moment were not within the auroral oval. Similarly, *Saroso et al.* [1992] compared the WDC AE with a southern polar cap index SAE, derived from four evenly spaced Antarctic magnetometer stations. The comparison results from this study are inconclusive, mostly because the southern stations were at higher magnetic latitude than the AE stations.

1.2.1. AE Interhemispheric Asymmetries

Recently, *Weygand and Zesta* [2008] conducted a study similar to that of *Maclennan et al.* [1991] and created an SAE index for comparison with the World Data Center (WDC) AE index for 7 days in December 2005. *Weygand and Zesta* [2008] used all seven available Southern Hemisphere stations at magnetic latitudes between −60° and −71°, so that both northern and southern stations

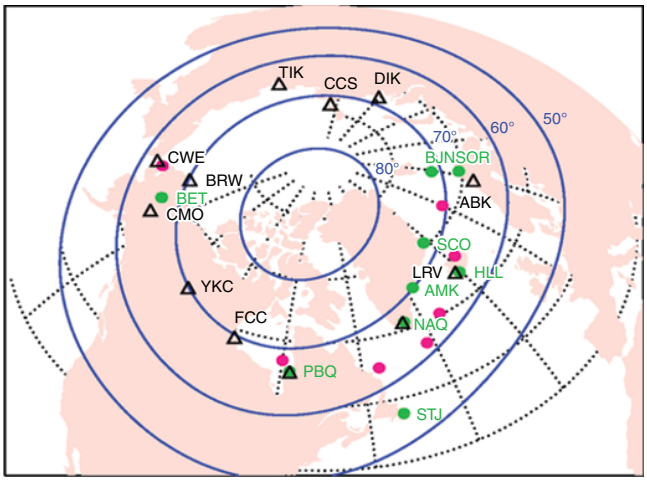

Figure 1.1 Map of northern and southern stations used for NAE and SAE calculations in *Weygand and Zesta* [2008]. In magenta are the north conjugate locations of the 7 southern stations for SAE, in green are the 9 northern stations for NAE, and the black triangles are the 12 standard AE stations.

were within the same topological region of the magnetosphere at the same time.

Figure 1.1 is a reproduction of Figure 2 from *Weygand and Zesta* [2008] and displays the location and distribution of all the Northern and Southern (projected to the north) hemisphere stations used for their study. The black triangles depict the standard AE stations, magenta solid circles are the north conjugate locations for the seven southern stations, as projected by the International Geomagnetic Reference Field (IGRF) model, and the green solid circles are northern stations selected for being as near conjugate as possible to the seven southern stations and are used to produce a northern AE (NAE) index conjugate to SAE. Black dotted lines are lines of geographic latitude and longitude and the solid blue lines are lines of constant geomagnetic latitude, calculated from Altitude Adjusted Corrected Geomagnetic Coordinate model [*Baker and Wing*, 1989]. The southern stations MAW, SYO, SNA, NVL, HBA, and WSD provide closely spaced coverage of a good portion of the auroral zone while MCQ station is farther away leaving a gap between WSD and MCQ and an even bigger gap from MCQ to MAW. The lack of similar coverage from the seven southern stations and the WDC AE stations is why *Weygand and Zesta* [2008] also created the conjugate NAE index from nine northern stations. There are more northern magnetometer stations than southern stations because exact conjugate stations are not always available. So, where necessary, data from the northern magnetometers that "surround" the conjugate southern station location are averaged together. For example, the conjugate signature for HBA (magenta circle immediately to the right of PBQ) is produced by averaging the data from NAQ, STJ, and PBQ. All the details of the different stations used and their coordinates are given in the original paper.

Figure 1.2 is reproduced from Figures 4 and 9 of *Weygand and Zesta* [2008] and shows the calculated indices for 10 December 2005 (an active day) on the top, and for 8 December 2005 (a quiet day) on the bottom. For each day, the AU, AL, and AE indices for the southern (SAE/AU/AL), conjugate Northern Hemisphere data (NAE/AU/AL), and the WDC indices are shown. The Northern Hemisphere indices are given in the top panels as solid black lines, and the Southern Hemisphere indices are shown in the bottom panels, also in solid black lines. The gray lines in the top panels are the WDC quick look indices that can stand in place of the standard AE, AU, and AL indices. In Figure 1.2a, only the first 12 hr of the day are available for 10 December 2005. There is good agreement between the northern indices and the WDC indices for the substorm just after 0600 UT visible in both NAE and AE. The correlation coefficient between AE and NAE is 0.86, which implies that activity is happening in local times where there is good coverage from southern stations (since the conjugate locations to the southern index are reproducing well the standard AE index) and the large gaps in coverage are not affecting this particular day. However, there is less agreement between the NAE and SAE indices, with a correlation coefficient of 0.69, which implies some real asymmetries between the Northern and Southern Hemispheres. The NAE and AE have clearly greater magnitude perturbations than the southern index, even though the event occurs during northern winter (low conductivity) and southern summer (high conductivity), when we expect stronger ionospheric currents in the Southern Hemisphere. The evidence therefore indicates the existence of significant asymmetries between the Northern and Southern hemisphere auroral electrojets, seemingly unrelated to seasonal variations and strong enough to overcome the expected seasonal asymmetries.

Figure 1.2b shows the northern and southern indices in the same format as in the previous event for a quiet day, 8 December 2005, and therefore the magnitude of the indices is significantly smaller. The black bar in each panel indicates the period of time when there is no station coverage in the local midnight sector for either SAE or NAE. For this event, there are significant differences between NAE and AE, particularly between 18 and 24 UT. In fact, the SAE index correlates much better with AE at that period of time, picking up the substorm activity at ~20 UT that is totally missed by NAE. Even for this very quiet day, there is strong evidence for interhemispheric asymmetries, likely due to IMF B_y.

It is likely that the interhemispheric currents, which have been theoretically postulated [*Benkevich et al.*, 2000; *Lyatskaya et al.*, 2014a, 2014b], contribute greatly to the

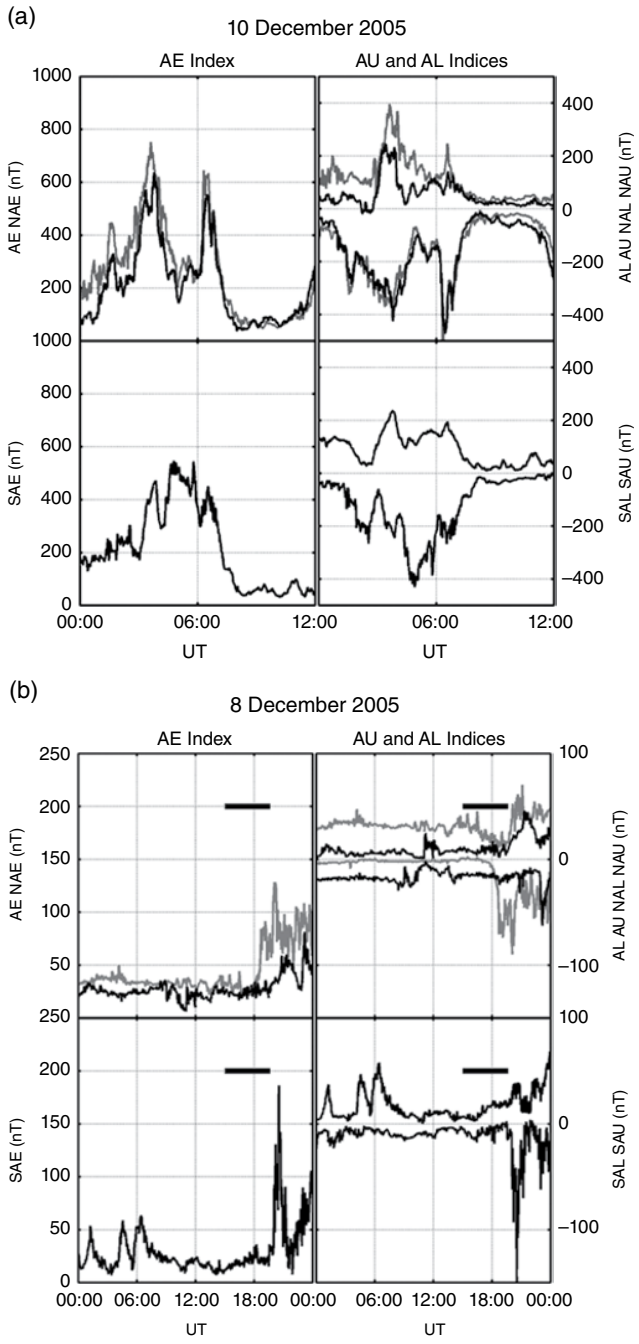

Figure 1.2 AE, NAE, and SAE calculations for (a) the active day on 10 December 2005, and (b) the quiet day on 8 December 2005. The black lines in top and bottom panels are the NAE/NAU/NAL and SAE/SAU/SAL indices, respectively, while the gray lines on the top panels are the standard AE/AU/AL indices.

observed asymmetries. *Weygand and Zesta* [2008] showed that the maximum north-south magnitude differences in the ground magnetic perturbations are seen in the local midnight region and are likely due to interhemispheric asymmetries of the nightside westward electroject. By extension, they suggested that when the local midnight region is well covered by stations in Antarctica, then the NAE can reasonably represent the WDC AE and then differences between NAE and SAE reasonably represent interhemispheric asymmetries in the auroral electrojets. This now opens the way for significant advancement in interhemispheric studies and in the effects of such asymmetries in global simulations.

Weygand et al. [2014a] expanded on the work of *Weygand and Zesta* [2008] by conducting a large statistical study on the correlation between the SAE, NAE, and AE indices. *Weygand et al.* [2014a] used the most complete, to date, database of Southern Hemisphere auroral magnetometers from 2005 to 2010 and were able to calculate the NAE and SAE indices simultaneously for a total of 274 days. (The individual NAE and SAE indices were available for a significantly greater number of days in each case.). The station distribution used in *Weygand et al.* [2014a] is very similar to that of Figure 1.1 with some small changes.

Figures 1.3a and b are reproduced from Figures 10 and 12 of *Weygand et al.* [2014a] and demonstrate some fundamental statistical properties for the northern and southern indices, based on the 274 days of available observations. Figure 1.3a shows histograms of the daily correlation between the SAE and NAE indices (top panel) and their mean daily differences (bottom panel). The correlation distribution peaks at 0.8, but the mean of the distribution is 0.65 with a maximum of 0.98 and a minimum of −0.2. This implies that, statistically, Northern and Southern Hemispheres electrojets are well correlated in terms of the timing of their dynamic changes. However, since the distribution is widely spread, there are often times of significant interhemispheric asymmetries. *Weygand et al.* [2014a] showed that the highest correlations occur during spring and to a lesser degree at fall, while the lowest correlations occur during northern winter and summer, when the two hemispheres are very asymmetrically illuminated, so there is an observed seasonal effect. The low correlation values in the top panel of Figure 1.3a correspond to quiet geomagnetic activity, as was also shown by *Weygand and Zesta* [2008], because the linear correlation of a nearly flat line (no activity) with another flat line is nearly zero by definition. This is demonstrated more clearly in Figure 1.3b where the mean daily correlation coefficients between SAE-NAE and SAE-AE are plotted with respect to the daily mean of the SAE index on the top and bottom panels, respectively. The black dots are the individual daily means and the gray squares are means of SAE index bins for a bin size of 50 nT. The gray bars are the standard deviation of the means for each bin. The gray line is drawn as visual aid for the data trends. Low correlation coefficients are only associated with very low geomagnetic activity, while higher correlations exist for both quiet and active days. Highly active days have only higher correlation coefficients, >0.5.

The persistent magnitude difference between SAE and NAE indices demonstrated in Figure 1.3a, bottom panel,

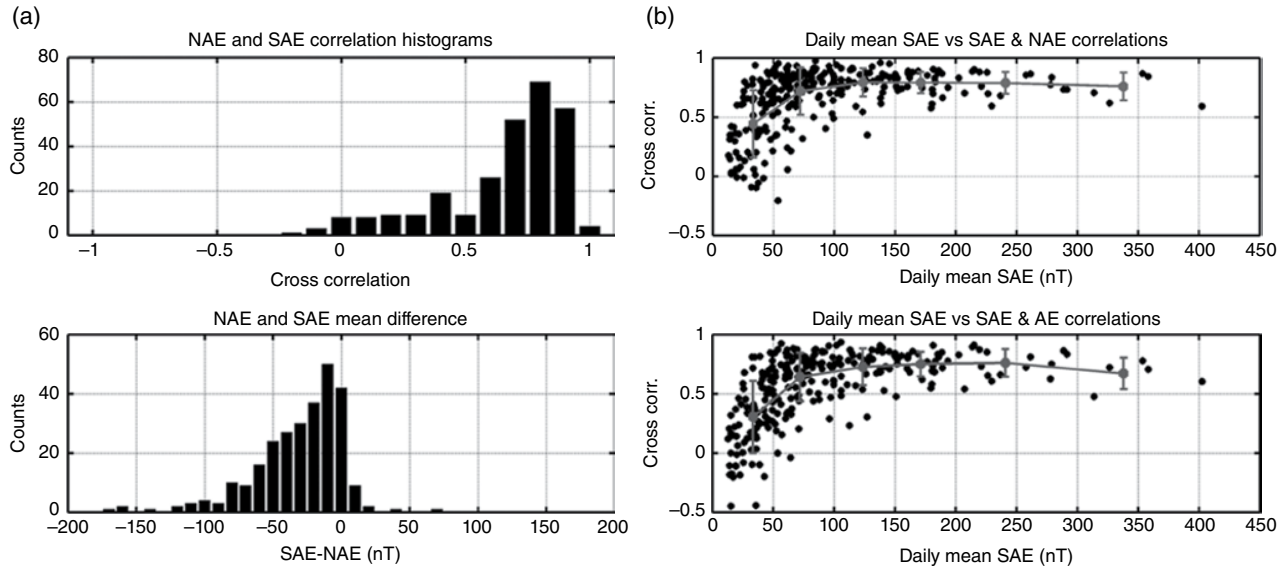

Figure 1.3 (a) Histograms of the SAE-NAE daily correlations (top) and of the SAE-NAE mean daily differences (bottom); (b) daily mean SAE-NAE correlation (top) and SAE-AE correlations (bottom) with respect to the daily mean SAE [from *Weygand et al.*, 2014a].

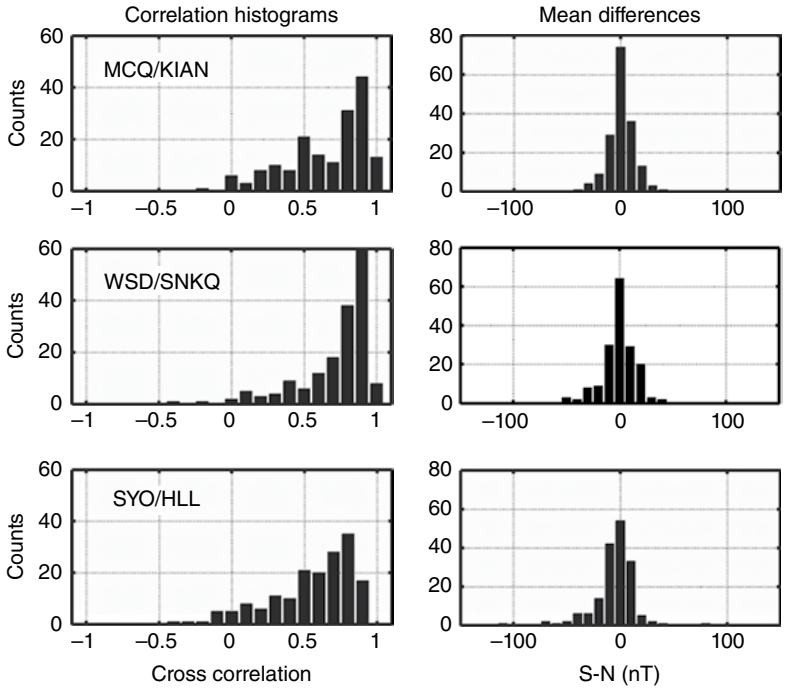

Figure 1.4 (Left) Histograms of the correlations between closely conjugate south-north pairs of stations MCQ-KIAN, WSD-SNKQ, and SYO-HLL, and (right) histograms of the difference between the *H* component for each pair of stations.

with SAE on average smaller than NAE was reported also by *Maclennan et al.* [1991] and seems to indicate that the northern auroral electrojets are consistently stronger than the southern auroral electrojets. Since this is not a physically intuitive result, *Weygand et al*. [2014a] explored this matter further by isolating north-south pairs of stations included in the SAE and NAE calculations with good and poor conjugacy.

Figure 1.4 is a reproduction of Figure 14 from *Weygand et al.* [2014a] and shows, on the left column, histograms of the daily correlation of the *H* magnetic field component for station pairs MCQ-KIAN, WSD-SNKQ, and SYO-HLL,

where the first part of each pair is a southern station and the second is the northern station. On the right column of Figure 1.4, the daily mean differences are shown for the same three pairs of stations. The correlation plots for all three pairs are very similar to the SAE-NAE correlation histogram shown in Figure 1.3a (top panel), with the correlations peaking at 0.9. However, the daily mean histograms for the three pairs in Figure 1.4 are significantly different from the SAE-NAE daily mean in Figure 1.3a, bottom panel. The mean daily difference for the three conjugate pairs is centered at 0 nT. Even though there is a spread to the distribution and there are clearly times with large interhemispheric asymmetries, the histograms of Figure 1.4, right column, seems to indicate that there is no systematic asymmetry between the north and south electrojets. The distributions of Figure 1.4 were produced with daily averaged values of north-south amplitude differences and for all different conditions. In Figure 1.5, we plot histogram distributions of the amplitude differences for the same three pairs of closely conjugate stations, but for 1 min averaged differences observed only in the local midnight region, ±3 hr around 00 MLT. The differences between north and south responses to the electrojet for low Kp are similar to those in Figure 1.4, namely centered around 0 and denoting no obvious systematic asymmetry between Northern and Southern Hemispheres. The histograms for high Kp values, however, show that for two of the three pairs, MCQ/KIAN and SYO/HLL, the peak is negative, indicating persistent stronger amplitudes at the northern stations. The third pair, WSD/SNKQ, has stations located in significantly different geographic latitudes.

The electrojet indices (AE, SAE, or NAE) are sensitive to the global DP2 current system, namely the global-scale two-cell convection pattern [*Nishida*, 1968], but are also most strongly sensitive to the nightside westward electrojet that is typically the result of substorm or other strong activity, known as the DP1 current system [*Nishida*, 1968]. One then would expect most of the interhemispheric asymmetries in the north and south indices to also be strongly sensitive to the nightside westward electrojet.

Figure 1.6 is a reproduction of Figure 17 from *Weygand et al.* [2014a] and demonstrates exactly this point. Figure 1.6 shows a superposed epoch analysis of the SAE-NAE differences on the top panel, and the difference in the *H* component between the south and north stations of the closely conjugate pairs that were discussed in Figure 1.4 and from all available data in the bottom three panels. For each pair of stations, the black line is the median and the two gray curves are the upper and lower quartiles of the distribution. The open circle in each panel indicates local midnight and the solid circle indicates local noon for that pair of stations. While the median curve varies minimally, it is clear from the quartile curves that the largest differences between the north and south stations of the pair occur around local midnight and are therefore associated with the nightside westward electrojet. We therefore propose that for times when there is good coverage of the local midnight region from the

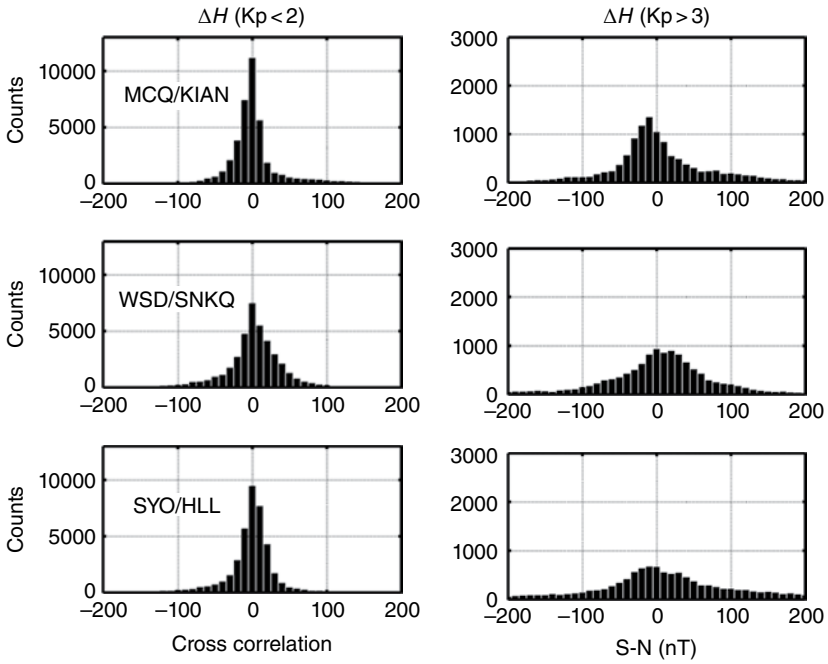

Figure 1.5 Histograms of the *H* component differences for the same three pairs of closely conjugate stations as in Figure 1.4. On the left are the histograms for low geomagnetic activity (Kp < 2) and on the right are the histograms for high geomagnetic activity (Kp > 3).

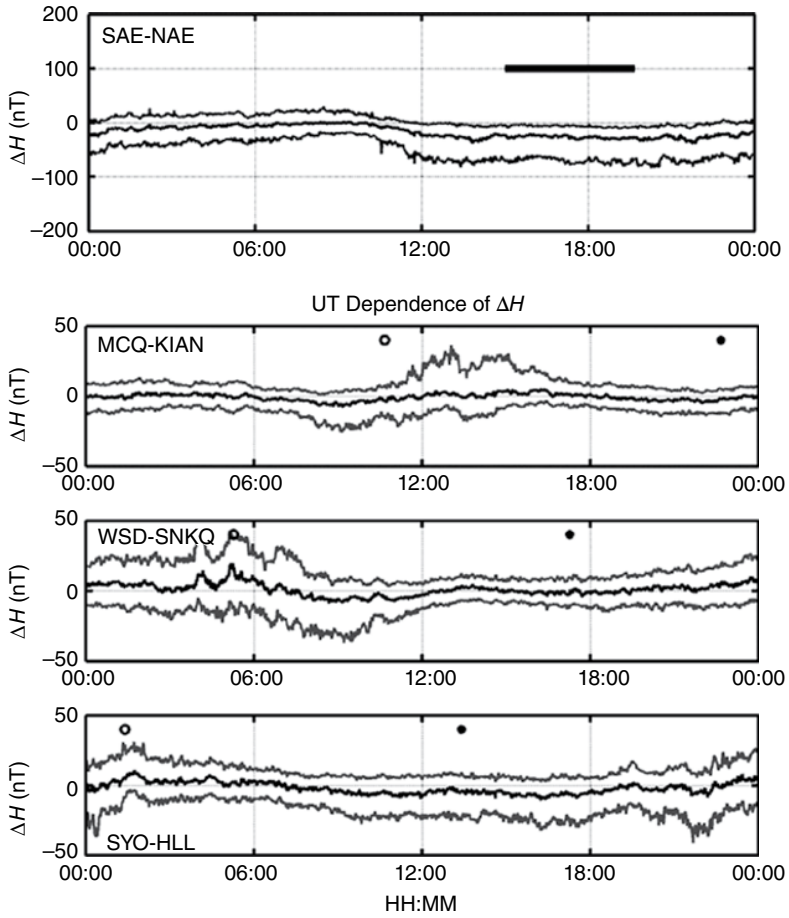

Figure 1.6 (Top panel) Superposed epoch UT dependence of the SAE-NAE differences, solid line. The lighter shade lines are the upper and lower quartiles of the distribution. (Panels 2–4) Superposed epoch of the difference in the *H* component for the same three closely conjugate pairs of ground magnetometer stations of Figure 1.4. The station pairs are given on the left side of the panel; the open circles indicate local midnight for each station, and the filled circles indicate local noon. Upper and lower distribution quartiles are shown in lighter shade lines around the main distribution.

Southern Hemisphere, the SAE can be used as the equivalent Southern Hemisphere Auroral Electrojet index.

Most important, Figure 1.6, in combination with the histograms of Figure 1.5, gives an insight into possible reasons for the systematic asymmetry between SAE and NAE from Figure 1.3a. The negative SAE-NAE distribution peak is manifested in the 12–24 UT period, which engulfs the time period when no southern stations are in near local midnight (indicated by the horizontal bar), where most of the amplitude and differences in SAE and NAE originate. The longitudinal distribution of stations is clearly a contributor to the observed systematic asymmetry between SAE and NAE. The UT differences of the *H* component for the three pairs in Figure 1.6 demonstrate another important point. While the daily averaged differences may be centered at 0 (Fig. 1.4), the distributions can be systematically positive or negative during the day. This and the systematic differences for higher geomagnetic activity in Figure 1.5 indicate that the SAE/NAE systematic asymmetry is not due just to the longitudinal gaps in the Southern Hemisphere, but also to other factors like the geographic differences between station pairs, interhemispheric currents, or activity levels.

While the precise causes of the observed north-south asymmetry in SAE and NAE remain unclear, the spread of the histogram distributions in Figures 1.4 and 1.5 demonstrate the significant interhemispheric asymmetries that habitually occur.

1.2.2. The Effect of Solar Wind and IMF on the Interhemispheric Asymmetries

We now look at the role the solar wind and IMF may play in the observed interhemispheric asymmetries as evidenced by the calculated SAE and NAE indices.

Specifically, we examine how different solar-wind parameters affect the correlation between the SAE and NAE indices.

For the solar-wind study, we recalculated cross correlation coefficients between the three AE indices (standard AE, NAE, and SAE) at a much faster cadence than was used in the *Weygand et al.* [2014a] work. We used our complete database, which amounts to 274 days, from December 2005 to August 2010, when all three indices are available. The cross correlation coefficients are estimated every 10 min with a correlation window of 2 hr around each point in time. The solar-wind and IMF quantities are taken from ACE data and are propagated to 17 R_E using the Weimer technique [*Weimer et al.*, 2003; *Weimer*, 2004]. In order to include propagation to the ionosphere and effects of preconditioning of the magnetosphere by previous solar wind and IMF values, we introduce two additional time constants: delay time, T_d, for the propagation to the ionosphere from 17 R_E, and preconditioning time, T_p, for averaging the solar wind and IMF data before each point. For T_d we use 10 min as an average propagation window from 17 R_E upstream to the ionosphere. For T_p we use 20 min and that is the time period beyond the 10 min (T_d) for which we average the SW parameters to get a sense of preconditioning. Therefore, each index correlation is assigned solar wind and IMF values by shifting the propagated ACE data by T_d minutes, and then averaging the solar-wind data for T_p minutes before that. With all the correlation coefficients calculated, a statistical study of the effects of solar wind and IMF conditions on the electrojet index correlations can be performed. While a more complete and focused manuscript is in preparation, we show here some key results of this new work. Specifically, we examine the effect of IMF B_y, IMF B_z, and solar-wind dynamic pressure, P_{sw} on the north-south index correlations.

Figure 1.7 shows the magnitude of the AE/SAE and NAE/SAE correlations as a function of IMF B_z and P_{sw}. The IMF and dynamic pressure data accompanying the correlation coefficients are binned at 1 nT and 0.25 nPa bins. In each bin, we plot the percentage of high-correlation coefficients ($R > 0.7$) that occur during the bin conditions. The "percentage of correlations" quantity was chosen over the average bin correlation coefficient because it shows the IMF and dynamic pressure dependence more clearly. It is clear that both the AE/SAE (left) and NAE/SAE (right) plots suggest strong dependence of the north/south correlations on IMF B_z and P_{sw}. The percentage of high coefficients is higher for southward IMF, and for steady IMF it increases with dynamic pressure. In other words, the more southward the IMF and the higher the dynamic pressure, the better correlated the north-south electrojets are, while more northward IMF and low dynamic pressure are more statistically likely to produce asymmetrical north and south electrojets. We should caution here that high correlations between north and south indices do not exclude high differences in amplitude between north and south, and future work will address all these issues. Both IMF B_z and high dynamic pressure can be strong drivers of geomagnetic activity, relocating magnetospheric population boundaries, enhancing large-scale field-aligned currents, enhancing convection in the magnetosphere and ionosphere, as well as ionospheric currents. Under strongly driven conditions, both SAE and NAE (or AE) would be characterized by distinct enhancements well correlated in time,

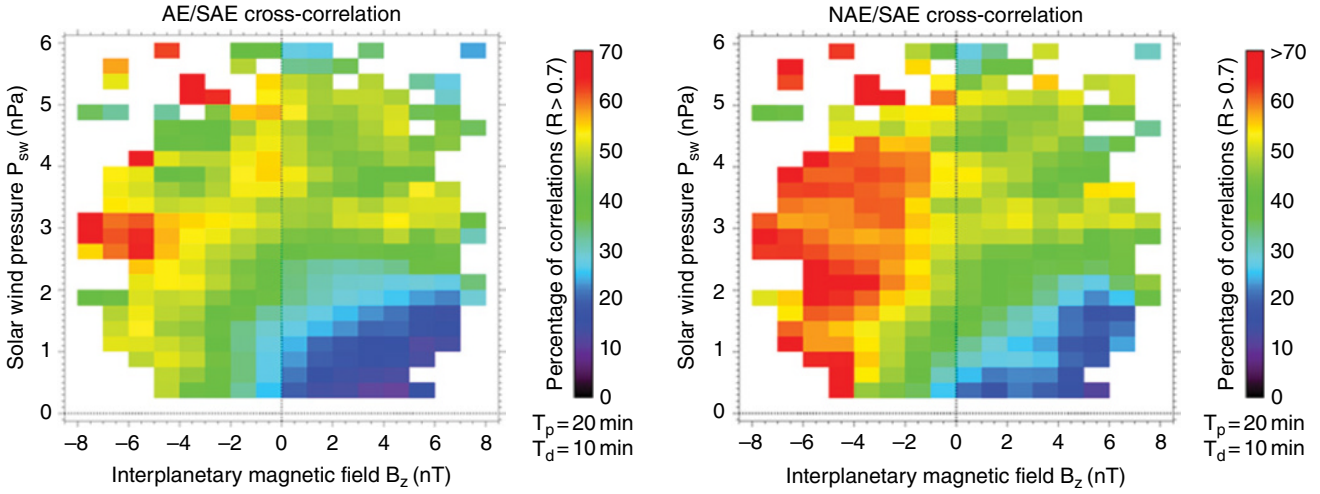

Figure 1.7 (Left) AE/SAE and (right) NAE/SAE correlation results as a function of ACE IMF B_z and solar wind dynamic pressure.

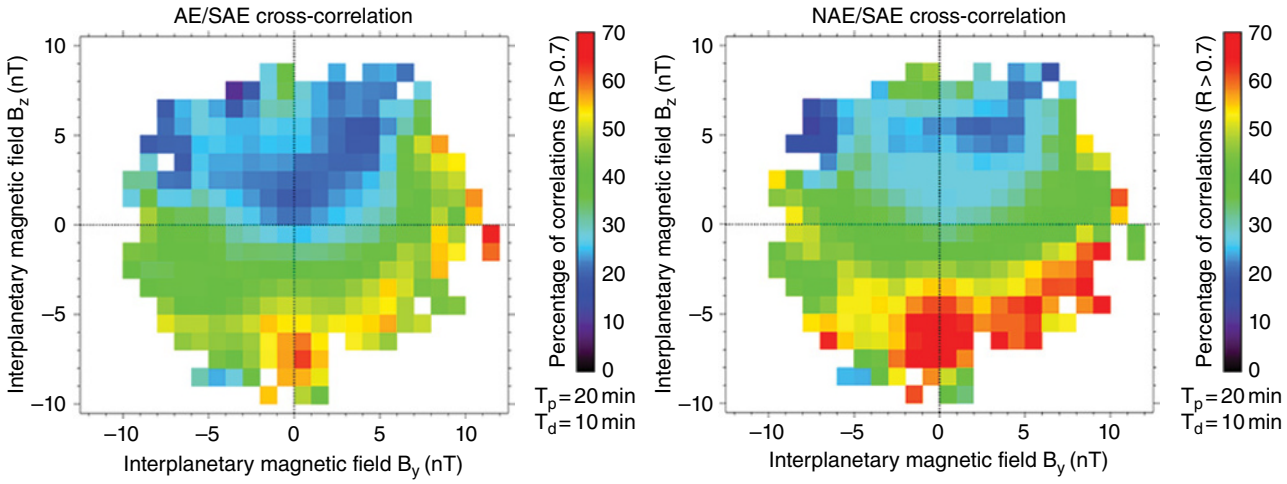

Figure 1.8 (Left) AE/SAE and (right) NAE/SAE correlation results as a function of ACE IMF B_y and B_z.

leading to high correlation coefficients even though their amplitude differences may not be necessarily small.

Figure 1.8 shows the dependence of the percentage of high correlations on the concurrent IMF B_y and B_z components. The IMF B_z dependence is again clear. In addition, high correlation coefficients appear for high absolute values of IMF B_y, even when the IMF is northward. Furthermore, high correlations seem to be present when the IMF is purely northward but with high magnitude; however, it is unclear if this is a real dependence or result of low statistics at these high northward IMF values. An asymmetry for positive and negative IMF B_y is also evident, mostly for southward IMF. We see stronger correlations for positive IMF B_y than for negative IMF B_y.

1.3. ULF WAVE POWER ASYMMETRIES

Ultra low frequency waves are the lowest frequency magnetohydrodynamic (MHD) waves generated in the magnetosphere in response to solar-wind drivers and internal dynamic processes. They are an excellent diagnostic tool that can determine and track the energy flow from the solar wind and through the different magnetospheric regions. They also provide a good way of understanding how magnetospheric processes couple down to the ionosphere and thermosphere. For example, *Yizengaw et al.* [2013] demonstrated that during a solar-wind high speed stream (HSS) event, upstream oscillations directly drove ULF waves globally within the magnetosphere, which also penetrated to the ionosphere at all latitudes and down to the equator where they drove similar oscillation in the equatorial electrojet and the measured ionospheric total electron content (TEC).

1.3.1. Prior Studies

Conjugate studies of ULF waves can additionally provide information on how the flow of energy from the solar wind is distributed to the two hemispheres, but unfortunately such prior studies are few and far between.

Most of the conjugate studies on ULF pulsations have been done at high latitudes and the cusp. *Ables et al.* [2000] and *Liu et al.* [2003] studied resonant Pc5 waves with high conjugacy to determine IMF dependencies, *Matthews et al.* [1996] used both ground magnetometers and radar observations to study the conjugate wave response to a solar-wind shock impact, and *Posch et al.* [1999] looked at conjugate asymmetries of broadband (0–50 mHz) waves.

Conjugate wave studies from lower latitudes are just as uncommon as high-latitude studies. A series of publications looked at various aspects of conjugacy in Pc4-5 waves near L = 4, using magnetometer data from Siple station in Antarctica and a set of three near conjugate stations from the north. *Lanzerotti et al.* [1973] and *Surkan and Lanzerotti* [1974] looked at the conjugate wave power at quiet and disturbed conditions, respectively, during the 1971 December solstice. They found that during quiet days the ratio of south to north wave power was ~1, but for disturbed days the wave power was much stronger in the southern station, which is opposite to what we are reporting here, but they examined higher latitudes. *Feng et al.* [1995] studied conjugate Pc3-4 pulsations at low latitude, L = 1.2, and while they did not report on the relative wave power between the north and south stations, they found evidence that the observed waves were due to resonances and their daily occurrence pattern is controlled by their source and propagation characteristics.

Obana et al. [2005] studied the north-south asymmetry of Pc3-5 waves at higher latitudes with a pair of conjugate stations at L = 5.4. While the latitude of the conjugate observations is much higher than the low-latitude and midlatitude station pairs we are including in our study, the *Obana et al.* [2005] work is the only other work that directly looks at the wave-power ratio between the two hemispheres. They found a seasonal variation in the north vs. south power ratio and also found that the power in the northern station is always higher than at the southern stations throughout the year, as we report here. They named that the "positive effect." They considered ionospheric conductivity effects as the source for the observed seasonal asymmetries and differences in the magnitude of the background magnetic field to explain the positive effect. We provide more detailed comparisons in the section below.

1.3.2. Low Latitude and Midlatitude ULF Wave-Power Asymmetries

We performed a conjugate study of ULF wave power along the Americas meridian and we present here some key representative results. We utilized stations from three magnetometer chains: the South American Meridional B-field Array (SAMBA) [*Boudouridis and Zesta*, 2007], a chain of 12 magnetometers along Chile and in Antarctica, covering mostly low latitudes and midlatitudes, the Magnetometers along the Eastern Atlantic Seaboard for Undergraduate Research and Education (MEASURE) [*Berube et al.*, 2003], which has several stations along the East Coast of the United States, some of them being directly conjugate with SAMBA stations, and the Midcontinent Magnetoseismic Chain (McMAC) [*Chi et al.*, 2013], which extends the CARISMA (Canadian Array for Realtime Investigations of Magnetic Activity) Churchill line of magnetometers southward to Mexico at low latitudes. The McMAC meridian is approximately 2 hr of MLT separated by the average meridian of the MEASURE and SAMBA chains.

Figure 1.9 is a map of the magnetometer locations set in the Southern Hemisphere with the three Northern Hemisphere stations that we used projected to their magnetic conjugate points, using the appropriate epoch IGRF model. The dotted lines are lines of geographic latitude 10° apart, and geographic longitude 20° apart. The blue lines are lines of constant geomagnetic latitude from −10° to −60°. The southern SAMBA stations of PAC, OHI, and PAL are denoted as blue solid circles, while the northern stations of FIT and APL from MEASURE, and AMER from McMAC are red solid circles. FIT and PAC are approximately at L = 1.7, while the remaining stations are approximately at L = 2.3.

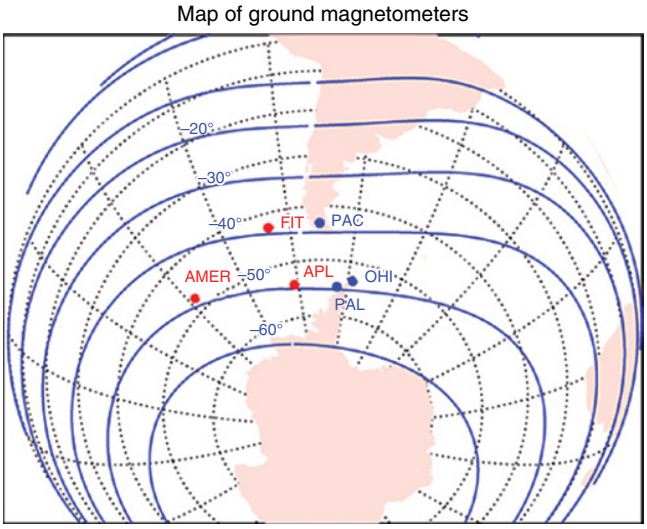

Figure 1.9 Map showing the southern and northern conjugate stations that were used for studying the north-south asymmetries of ULF wave power. In blue are the southern SAMBA stations, while in red are the conjugate projections of the northern MEASURE and McMAC stations.

For our comparisons of interhemispheric wave power and its seasonal and annual variations, we calculate the total daily power separately in the Pc3 (20–100 mHz) and Pc4-5 (2–20 mHz) bands for each station. The daily power calculation includes only the dayside, approximately 0630–1730 MLT, for each station. Pc3–Pc5 waves typically have different sources on the dayside and nightside and are regularly present and stronger on the dayside, resulting primarily from upstream sources and solar wind magnetosphere interactions [e.g., *Yumoto*, 1985; *Troitskaya and Bolshakova*, 1988]. Our station pairs are conjugate in latitude but can be separated in MLT by as little as a half hour, in the case of the FIT-PAC pair, or as much as 3 hr, in the case of the AMER-OHI pair. Since this is a statistical study with only daily values of dayside wave power, any instantaneous MLT differences between our conjugate pairs of stations do not influence our conclusions. We calculate the daily total power from the dynamic spectrum analysis from summed 1 min bins. We calculate the total power in all frequency bins every 1 min with a 10-min Fourier window centered on the minute of calculation. We continue moving our 10-min window to the subsequent slot until the full dayside period is covered and the total daily power is the sum of the power values of all the individual 1-min bins. We do this at each station and for the two frequency regimes, Pc3 and Pc4-5.

Figure 1.10 shows the results for the PAC-FIT pair of stations at L = 1.7 and for year 2005. The top panel shows the daily power for the north station FIT in red and for the south station PAC in blue. The bottom panel shows the ratio of the north to south station power (FIT-PAC).

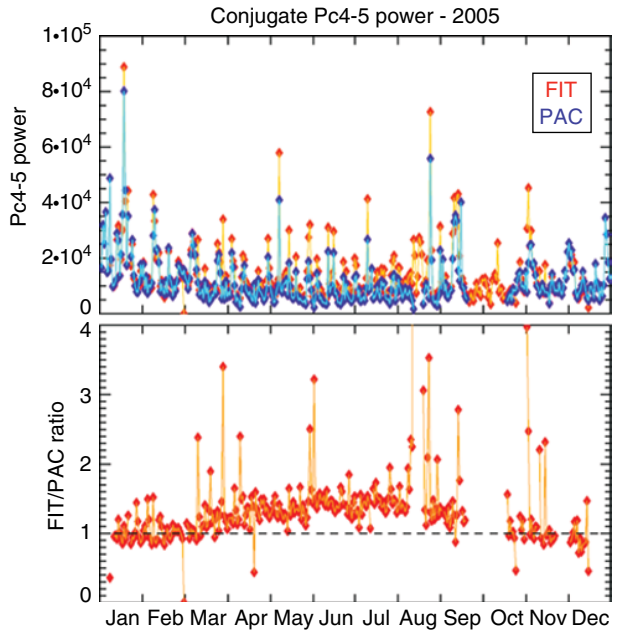

Figure 1.10 Conjugate Pc4-5 power at L = 1.7 for the FIT-PAC pair and for year 2005. The wave power for the north station FIT (red) and south station PAC (blue) is shown in the top panel, while the north-to-south power ratio is shown in the bottom panel.

A clear seasonal/annual variation is seen in the FIT-PAC ratio, with the ratio maximizing at June solstice (more illumination of the Northern Hemisphere) and minimizing at December solstice (less illumination of the Northern Hemisphere), which is intuitively expected by the ionospheric illumination patterns of the north and south hemispheres during the solstices. Most interesting, the December minimum of the FIT-PAC ratio is ~1, indicating similar wave power in the two hemispheres during December solstice, while the ratio maximum is ~1.5, indicating much stronger wave power in the north during June solstice. In short, there seems to be a Northern Hemisphere bias, in addition to the annual seasonal variation of wave power, with the northern station having consistently higher power than the southern station throughout the year.

This pattern observed in Figure 1.10 is consistent for both Pc3 and Pc4-5 bands and at both low-latitude (L = 1.7) and midlatitude (L = 2.3) conjugate stations. Figure 1.11 shows the daily Pc4-5 wave-power values for FIT on top and PAC on the bottom for year 2005 with polynomial fitted lines to demonstrate the annual variation of the data. We found that the best fit was a second order polynomial of the form $ax^2 + bx + c$, and it is shown

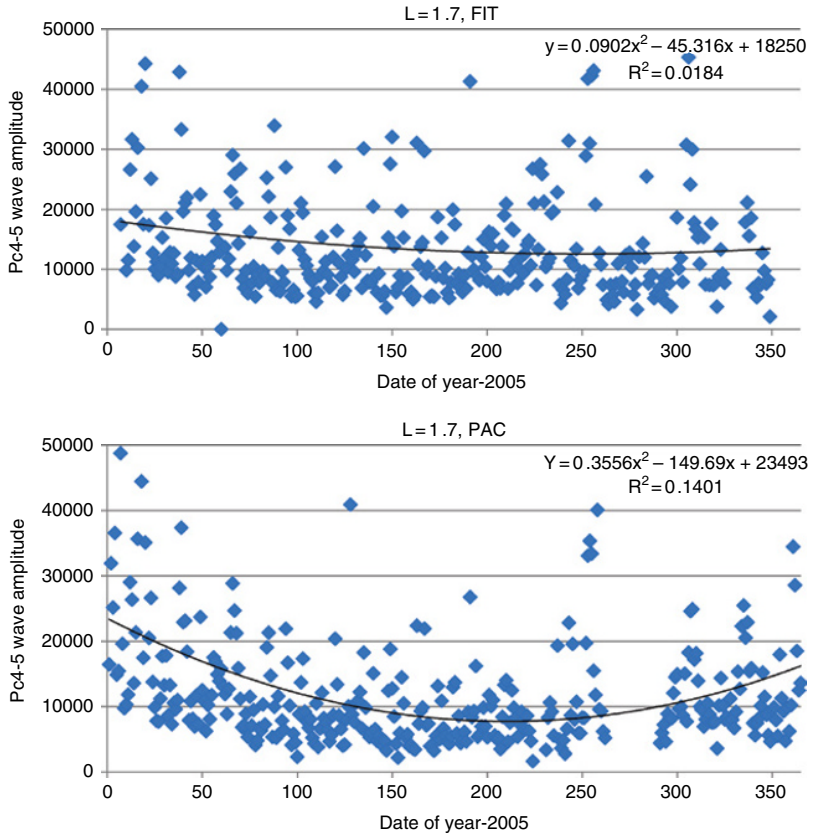

Figure 1.11 Annual distribution of the FIT and PAC daily wave power for 2005 and with second-order polynomial fits to demonstrate any seasonal trends.